Available online at www.sciencedirect.com
ScienceDirect
Journal of Sound and Vibration 311 (2008) 1391–1408
JOURNAL OF SOUND AND VIBRATION
www.elsevier.com/locate/jsvi

Active vibration suppression by pole-zero placement using measured receptances

John E. Mottershead[a,*], Maryam Ghandchi Tehrani[a], Simon James[a], Yitshak M. Ram[b]

[a]*Department of Engineering, University of Liverpool, Brownlow Hill, Liverpool L69 3GH, UK*
[b]*Department of Mechanical Engineering, Louisiana State University, Baton Rouge, USA*

Received 28 November 2006; received in revised form 15 October 2007; accepted 16 October 2007
Available online 26 November 2007

Abstract

The paper addresses the problem of pole-zero assignment using the receptance method in active vibration control and has applications particularly in vibration absorption and detuning of structures to avoid resonance. An output feedback approach is described that makes use of measured receptances, there being no requirement at all for the **M**, **C**, **K** matrices usually obtained by finite elements. Therefore, in the controller design, the approximations, assumptions and other modelling errors are largely eliminated. In addition, the method does not require the use of model reduction techniques or the estimation of unmeasured states by an observer. An advantage of the output feedback method, over state feedback, is that collocated actuator–sensor arrangements become possible. However this is achieved at the expense of creating characteristic equations nonlinear in the control gains. Numerical examples are provided to illustrate the working of the method. This is followed by a series of experimental tests carried out using collocated accelerometers and inertial actuators on a T-shaped plate. In a series of experiments poles and zeros are assigned separately and simultaneously. Stability robustness is demonstrated by applying a constraint to the singular values of the matrix return difference.

1. Introduction

The problem of eigenvalue assignment was studied quite extensively within the active control community during the 1970s and 1980s. Wonham [1] had shown in 1967 that if a system was controllable, then its eigenvalues (or poles) could be assigned by appropriate choice of *state* feedback. Davison [2] determined the conditions under which *output* feedback could be applied for eigenvalue assignment. Kimura [3] studied the problem of incomplete state observation and Moore [4] considered the freedom offered by state feedback beyond the specification of distinct closed-loop eigenvalues. Kautsky et al. [5] described numerical methods for determining robust (well conditioned) solutions to the state-feedback pole-assignment problem by defining a solution space of linearly independent eigenvectors, corresponding to the required eigenvalues. The solutions obtained were such that the sensitivity of assigned poles to perturbations in the system and gain

*Corresponding author.
E-mail address: j.e.mottershead@liverpool.ac.uk (J.E. Mottershead).

0022-460X/$ - see front matter © 2007 Elsevier Ltd. All rights reserved.
doi:10.1016/j.jsv.2007.10.024

matrices was minimised. More recently, Datta et al. [6] developed the closed-form solution for the partial pole-assignment problem where some desired eigenvalues were relocated while keeping all the other eigenvalues unchanged.

In vibration analysis the purpose of assigning poles and zeros is to suppress vibration. Examples include, moving poles further to the left-hand side of the complex plane to increase damping; assigning a zero at the tuned frequency of a classical vibration absorber; and moving natural frequencies away from resonance with applied harmonic loads by applying a passive structural modification. There are in fact numerous examples of structures having natural frequencies close to fixed excitation frequencies. Recently much attention has been focussed on inverse eigenvalue problems for assigning natural frequencies and mode shapes [7], vibration nodes [8] and anti-resonances [9] by structural modification. For example Mottershead et al. [10,11] measured rotational receptances and applied them to assign the natural frequencies and anti-resonances of a Γ-shaped structure by means of an added beam. Mottershead and Tehrani [12] carried out the structural modification of a helicopter tailcone also using measured rotational receptances obtained by means of an X-block attachment. Mottershead and Ram [13] reviewed the field of inverse eigenvalue problems for vibration absorption by structural modification and active control. The advantage of the structural modification approach is that the system is guaranteed to remain stable. However there are very considerable disadvantages: (1) the form of the modification that can be realised physically (symmetry, positive-definiteness, pattern of non-zero matrix terms) is restrictive, (2) rotational receptances are very difficult to measure and require high levels of specialist expertise, and (3) the number of eigenvalues to be assigned must be matched by the rank of the modification.

In recent times many of the disadvantages that prevented the practical application of active control to flexible structures, with low damping and large numbers of modes, have been overcome. Inertial actuators for the application of 'sky-hook' damping [14] and piezo-electric devices [15] for thin plate-like applications have been developed. Active damping by velocity feedback has received much attention recently. A good example is the 'smart panel' described by Gardonio et al. in a three-part paper [16–18] covering the theory, design and application of the system, which comprised 16 decentralised units for the control of sound transmission. Each control unit consisted of a collocated accelerometer-sensor and a piezoceramic patch actuator with a single channel velocity feedback controller to generate active damping. A different approach, active constrained layer damping [19], can be particularly helpful in damping the higher-frequency closed-loop modes that might otherwise become unstable due to spillover [20].

The state-of-art in structural vibration control however is the 'independent modal-space control' method developed by Meirovitch and his students and described in the book 'Dynamics and Control of Structures' [21]. This approach allows in principle for the control of one structural mode independently of the others. In practice, the control force must be applied in the physical coordinates, which means that sufficient actuators must be used to ensure that the selected mode is controllable while the others are unaffected by the control force. Modern distributed actuators may be designed so that the vibration modes of a plate are controlled selectively in this way [22], but these techniques are not applicable to large-scale built-up structures consisting of many components. Meirovitch's analysis is presented in terms of the physical mass, damping and stiffness, $\mathbf{M}$, $\mathbf{C}$, $\mathbf{K}$, matrices finally arranged in the form of first-order state-space equations (when general viscous damping is included). From the point of view of the structural dynamics it is preferable to work with the second-order matrix pencil [23]. Redefining the second-order equations of motion into a first-order realisation destroys the desirable physical matrix properties of symmetry, definiteness and bandedness, and consequently the first-order state-space model does not preserve any notion of the second-order nature of the system.

In most cases the $\mathbf{M}$, $\mathbf{C}$, $\mathbf{K}$ matrices are obtained by finite elements, and may include the representation of distributed piezo-electric actuators and sensors, as described for example by Lim et al. [24]. Another way of implementing the independent modal-space control of Meirovitch is to use modal test data, derived from measured receptances, as described by Stobener and Gaul [25] in the active vibration control of a car body. Rayleigh (proportional) damping was assumed. An alternative approach that uses the measured receptances directly and makes no assumption about damping was proposed by Ram and Mottershead [26]. They showed, in principle, how state-feedback control using measured receptances from the original (open-loop) system could be used to assign all the poles of the closed-loop system using just a single actuator. Additionally, this method preserved the second-order nature of the physical system since the receptances are given by, $\mathbf{H}(\mathrm{i}\omega) = (-\omega^2\mathbf{M} + \mathrm{i}\omega\mathbf{C} + \mathbf{K})^{-1}$ and the poles and zeros (anti-resonances) were assigned without the need to

know or evaluate the **M**, **C**, **K** matrices. A further significant point is that the familiar state-space approach requires a dynamic stiffness model and all the states must be measured, or estimated using an observer, in order to make the system equations complete. On the other hand, when using the receptance method only the available states are needed to complete the equations. This means that by the receptance method there is no need to estimate the unmeasured states using an observer. Neither is there any need for model reduction.

In this paper the receptance method for output-feedback is described in detail. The very considerable advantage of the output feedback method over state feedback is that it allows the use of collocated actuators and sensors in multiple-input–multiple-output (MIMO) systems. It is well known that the transfer function of a lightly damped system with a collocated actuator–sensor pair displays a line of interlacing poles and zeros just to the left of the imaginary axis. The benefits of this arrangement were discussed in detail by Preumont [27] who showed the trajectory of one such pole to be into the left-hand half-plane, therefore remaining stable under closed-loop control. In addition to velocity feedback, for active damping, the method uses displacement feedback for active stiffness, thereby enabling the assignment of both poles and zeros to desired locations in the complex s-plane. The assignment of zeros is of special interest in vibration analysis because the vibration can be made to vanish at chosen frequencies and locations. Active stiffness is more difficult to achieve than active damping [28] as can be appreciated when considering the location of a modal circle on the Nyquist diagram. In the case of velocity feedback the modal circle is confined to the right-hand half of the diagram, whereas for displacement feedback the circle occupies the lower two quadrants and can therefore be very close to the threshold of instability at -1. The method, described in the following section, is applied to both numerical and experimental examples. Three experiments on a 'T'-shaped plate are described. In the first experiment, four poles are assigned, and in the second, two zeros are assigned, each to the two-point-receptances corresponding to the locations of collocated proof-mass actuators and accelerometers. In the third experiment poles and zeros are assigned simultaneously. In all the experiments, the other poles of the system at higher frequencies are found to remain stable.

2. Poles and zeros

The dynamical equations, in the Laplace frequency domain, may be cast in the form of the second-order matrix equation,

$$(s^2\mathbf{M} + s\mathbf{C} + \mathbf{K})x(s) = \mathbf{B}\mathbf{u}(s) + \mathbf{p}(s), \tag{1}$$

where $\mathbf{M}, \mathbf{C}, \mathbf{K} \in \Re^{n\times n}$; $\mathbf{M} = \mathbf{M}^{\mathrm{T}}$; $\mathbf{C} = \mathbf{C}^{\mathrm{T}}$; $\mathbf{K} = \mathbf{K}^{\mathrm{T}}$; $\mathbf{M} > 0$; $\mathbf{C}, \mathbf{K} \geqslant 0$ are the usual structural stiffness, damping and mass matrices, $\mathbf{B} \in \Re^{n\times m}$ is the control force distribution matrix, $\mathbf{x}(s)$, $\mathbf{p}(s) \in \Re^{n\times 1}$ represent the displacement states and external forces, respectively, and $\mathbf{u}(s) \in \Re^{m\times 1}$ is the control force. Likewise, the output equation may be written as

$$\mathbf{y}(s) = \mathbf{D}\mathbf{x}(s), \tag{2}$$

where $\mathbf{D} \in \Re^{l\times n}$ is the sensor distribution matrix and the output is denoted by $\mathbf{y} \in \Re^{l\times 1}$. The feedback law is expressed as

$$\mathbf{u}(s) = -(\mathbf{G} + s\mathbf{F})\mathbf{y}(s), \tag{3}$$

so that the output and rate gains are given by the terms in the matrices $\mathbf{G},\mathbf{F} \in \Re^{m\times l}$.

Then, combining Eqs. (1)–(3) leads to,

$$(s^2\mathbf{M} + s\mathbf{C} + \mathbf{K} + \mathbf{B}(\mathbf{G} + s\mathbf{F})\mathbf{D})\mathbf{x}(s) = \mathbf{p}(s). \tag{4}$$

Our purpose is to assign poles λ_j of the closed-loop system determined by the solution of,

$$\det\left(\lambda_j^2\mathbf{M} + \lambda_j(\mathbf{C} + \mathbf{BFD}) + (\mathbf{K} + \mathbf{BGD})\right) = 0, \quad j = 1, 2, \ldots, r, \quad r \leqslant 2n \tag{5}$$

which we assume to be distinct and closed under conjugation. A necessary and sufficient condition is that the matrices **M**, $(\mathbf{C} + \mathbf{BFD})$ and $(\mathbf{K} + \mathbf{BGD})$ should be real.

The closed-loop zeros, μ_k, of the ppth point receptance, denoted $h_{pp}(s)$, are given by the solution of a different eigenvalue problem,

$$\det\left(\mu_k^2\mathbf{M}_p + \mu_k(\mathbf{C}+\mathbf{BFD})_p + (\mathbf{K}+\mathbf{BGD})_p\right) = 0, \tag{6}$$

where $\mathbf{M}_p$ is the submatrix corresponding to the ppth term of $\mathbf{M}$. Thus,

$$\mathbf{M} = \begin{bmatrix} m_{pp} & \mathbf{m}_p^{\mathrm{T}} \\ \mathbf{m}_p & \mathbf{M}_p \end{bmatrix}, \quad \mathbf{m}_p^{\mathrm{T}} = \begin{bmatrix} m_{p1} & \cdots & m_{p,p-1} & m_{p,p+1} & \cdots & m_{pn} \end{bmatrix} \tag{7,8}$$

and

$$\mathbf{M}_p = \begin{bmatrix} m_{11} & \cdots & m_{1,p-1} & m_{1,p+1} & \cdots & m_{1n} \\ \vdots & & \vdots & \vdots & & \vdots \\ m_{p-1,1} & \cdots & m_{p-1,p-1} & m_{p-1,p+1} & \cdots & m_{p-1,n} \\ m_{p+1,1} & \cdots & m_{p+1,p-1} & m_{p+1,p+1} & \cdots & m_{p+1,n} \\ \vdots & & \vdots & \vdots & & \vdots \\ m_{n1} & \cdots & m_{n,p-1} & m_{n,p+1} & \cdots & m_{nn} \end{bmatrix} \tag{9}$$

with similar definitions for the submatrices $(\mathbf{C}+\mathbf{BFD})_p$ and $(\mathbf{K}+\mathbf{BGD})_p$. It is seen that the zeros are the eigenvalues of the system grounded at the pth coordinate. As with the poles, we assume the zeros to be distinct and closed under conjugation.

3. Pole and zero assignment by using receptances

The receptance matrix of the open-loop system is now defined as

$$\mathbf{H}(s) = (s^2\mathbf{M} + s\mathbf{C} + \mathbf{K})^{-1}. \tag{10}$$

Premultiplying both sides of Eq. (4) by $\mathbf{H}(s)$ then gives,

$$(\mathbf{I} + \mathbf{H}(s)\Delta\mathbf{Z}(s))\mathbf{x}(s) = \mathbf{H}(s)\mathbf{p}(s), \tag{11}$$

where

$$\Delta\mathbf{Z}(s) = \mathbf{B}(\mathbf{G} + s\mathbf{F})\mathbf{D} \tag{12}$$

and finally the closed-loop receptance equation can be expressed in terms of the open-loop receptances as

$$\mathbf{x}(s) = (\mathbf{I} + \mathbf{H}(s)\mathbf{B}(\mathbf{G} + s\mathbf{F})\mathbf{D})^{-1}\mathbf{H}(s)\mathbf{p}(s) \tag{13}$$

or

$$\mathbf{x}(s) = \frac{\mathrm{adj}(\mathbf{I} + \mathbf{H}(s)\mathbf{B}(\mathbf{G} + s\mathbf{F})\mathbf{D})}{\det(\mathbf{I} + \mathbf{H}(s)\mathbf{B}(\mathbf{G} + s\mathbf{F})\mathbf{D})}\mathbf{H}(s)\mathbf{p}(s). \tag{14}$$

The closed-loop system poles may be assigned by selecting real-valued gains $\mathbf{G}$, $\mathbf{F}$, to satisfy the nonlinear characteristic equations,

$$\det\left(\mathbf{I} + \mathbf{H}(\lambda_j)\mathbf{B}(\mathbf{G} + \lambda_j\mathbf{F})\mathbf{D}\right) = 0, \quad j = 1, 2, \ldots, r, \quad r \leqslant 2n, \tag{15}$$

where the assigned poles are distinct and closed under conjugation. Since the equations are nonlinear in the gains there may be one or more strictly real solutions $\mathbf{G}$, $\mathbf{F}$ or there may be no solution, in which case the closed-loop system is uncontrollable.

The zeros of the closed-loop system occur when terms in the numerator matrix product, $\mathrm{adj}(\mathbf{I}+\mathbf{H}(s)\mathbf{B}(\mathbf{G}+s\mathbf{F})\mathbf{D})\mathbf{H}(s)$, vanish to zero. The zeros of the ppth receptance may therefore be assigned by selecting gains such that,

$$\left[\mathrm{adj}\left(\mathbf{I} + \mathbf{H}(\mu_k)\mathbf{B}(\mathbf{G} + \mu_k\mathbf{F})\mathbf{D}\right)\mathbf{H}(\mu_k)\right]_{pp} = 0. \tag{16}$$

We consider zeros that are distinct and closed under conjugation, so that if a solution (or solutions) exist then the gains are found to be strictly real.

If the sensors and actuators are collocated,

$$\mathbf{D} = \mathbf{B}^{\mathrm{T}} \in \Re^{m\times n} \tag{17}$$

and the gain matrices are symmetric and positive semi-definite,

$$\mathbf{G} = \mathbf{G}^{\mathrm{T}} \in \Re^{m\times m}, \quad \mathbf{F} = \mathbf{F}^{\mathrm{T}} \in \Re^{m\times m}, \quad \mathbf{G},\ \mathbf{F} \geqslant 0, \tag{18}$$

then it is seen from Eq. (5) that the closed-loop system matrices are symmetric with unchanged definiteness properties, which means that the poles have strictly negative real parts. In practice the actuator and sensor dynamics, neglected in the above theory, must be considered, as indeed they are in the experimental study that follows in Section 5. The use of collocated actuator–sensor systems was discussed in detail by Preumont [27].

The resulting characteristic equations (Eqs. (5) and (6) combined with Eqs. (17) and (18)) retain considerably greater freedom in the choice of control gains than does a passive structural modification by the adjustment of physical parameters such as beam cross sections or added masses.

In the following numerical and experimental examples the gain matrices are diagonal,

$$\mathbf{F} = \mathrm{diag}(f_i), \quad \mathbf{G} = \mathrm{diag}(g_i), \quad i = 1, 2, \ldots, m. \tag{19}$$

This is perhaps the simplest form for the gain matrices, but it should be noted that in more complex or larger structural problems there may be advantages in retaining the fully populated symmetric form of Eqs. (18). In principle, the fully populated matrices should allow more poles and zeros to be assigned than the number of actuators and sensors. Alternatively, a greater number of solutions to the nonlinear characteristic equations may become available, thereby allowing the selection of gains that result in the least cost of control or that render those assigned poles and zeros least sensitive to small changes in the gain terms.

4. Numerical examples

The method is illustrated by a series of eigenvalue assignment exercises based upon the system shown in Fig. 1. The parameters of the system have the following values: $k_1 = 3$, $k_2 = 2$, $k_3 = 2$, $k_4 = 1$, $c_1 = 0.1$, $c_2 = 0.1$, $m_1 = 2$, $m_2 = 1$, $m_3 = 3$.

Example 1 (*Assignment of poles*). Two pairs of complex conjugate poles at $\lambda_{1,2} = -0.01 \pm 0.7\mathrm{i}$ and $\lambda_{3,4} = -0.06 \pm 1.8\mathrm{i}$ are assigned using two actuators supplying feedback control forces at masses m_1 and m_3.

The mass, damping and stiffness matrices are given by

$$\mathbf{M} = \begin{bmatrix} 2 & 0 & 0 \\ 0 & 1 & 0 \\ 0 & 0 & 3 \end{bmatrix}, \quad \mathbf{C} = \begin{bmatrix} 0.1 & 0 & 0 \\ 0 & 0.1 & -0.1 \\ 0 & -0.1 & 0.1 \end{bmatrix}, \quad \mathbf{K} = \begin{bmatrix} 6 & -2 & -1 \\ -2 & 4 & -2 \\ -1 & -2 & 3 \end{bmatrix}$$

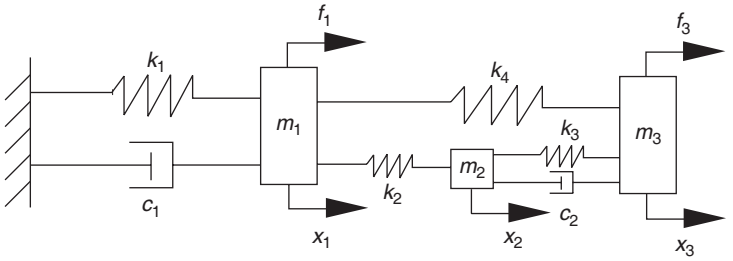

Fig. 1. Three degree-of-freedom system.

and the matrices **B** and **D** are chosen to be,

$$\mathbf{D} = \mathbf{B}^{\mathrm{T}} = \begin{bmatrix} 1 & 0 & 0 \\ 0 & 0 & 1 \end{bmatrix},$$

so that $y_1 = x_1$, $y_2 = x_3$.

The open-loop system receptances are at the values of s corresponding to the chosen eigenvalues,

$$\mathbf{H}(\lambda_j) = \left(\mathbf{M}\lambda_j^2 + \mathbf{C}\lambda_j + \mathbf{K}\right)^{-1}, \quad j = 1, \ldots, 4.$$

Four characteristic equations (17), generally nonlinear in the gains, g_i, f_i, are then solved numerically using a Gauss–Newton method,

$$\det\left(\mathbf{I} - \mathbf{H}(\lambda_{\mathrm{j}})\mathbf{B}\,\mathrm{diag}\left(f_i + \lambda_j g_i\right)\mathbf{B}^{\mathrm{T}}\right) = 0, \quad j = 1, \ldots, 4$$

with the result that,

$$\mathbf{F} = \mathrm{diag}(0.0999, 0.0475), \quad \mathbf{G} = \mathrm{diag}(2.3873, 0.3401).$$

In order to validate the results, the eigenvalues of the closed-loop system are obtained by the state-space method,

$$\mathbf{A} = \begin{bmatrix} \mathbf{0} & \mathbf{I} \\ -\mathbf{M}^{-1}(\mathbf{K} + \mathbf{B}\,\mathrm{diag}(g_i)\mathbf{B}^{\mathrm{T}}) & -\mathbf{M}^{-1}(\mathbf{C} + \mathbf{B}\,\mathrm{diag}(f_i)\mathbf{B}^{\mathrm{T}}) \end{bmatrix},$$

where

$$(\mathbf{C} + \mathbf{B}\,\mathrm{diag}(f_i)\mathbf{B}^{\mathrm{T}}) = \begin{bmatrix} 0.1999 & 0 & 0 \\ 0 & 0.1 & -0.1 \\ 0 & -0.1 & 0.1475 \end{bmatrix}$$

and

$$(\mathbf{K} + \mathbf{B}\,\mathrm{diag}(g_i)\mathbf{B}^{\mathrm{T}}) = \begin{bmatrix} 8.3873 & -2 & -1 \\ -2 & 4 & -2 \\ -1 & -2 & 3.3401 \end{bmatrix}$$

which yields the following poles:

$$\begin{aligned} \lambda_{1,2} &= -0.0100 \pm 0.7000\mathrm{i}, \\ \lambda_{3,4} &= -0.0600 \pm 1.8000\mathrm{i}, \\ \lambda_{5,6} &= -0.0546 \pm 2.3599\mathrm{i}. \end{aligned}$$

The first two pairs exactly replicate the values assigned and the third pair of poles are stable. The initial and modified receptances at m_1 are plotted in Fig. 2, represented by the solid (blue) and dashed (red) line, respectively.

Example 2 (*Assignment of zeros*). The zero assignment is considered for the point receptance h_{22}. Two pairs of complex conjugate zeros $\mu_{1,2} = -0.025 \pm 1.2\mathrm{i}$ and $\mu_{3,4} = -0.037 \pm 2\mathrm{i}$ are assigned using the feedback control forces at masses m_1 and m_3.

The sets of nonlinear equations (18) are solved to obtain the gains f_i and g_i

$$\left[\mathrm{adj}\left(\mathbf{I} + \mathbf{H}(\mu_j)\mathbf{B}\,\mathrm{diag}(g_i + \mu_j f_i)\mathbf{B}^{\mathrm{T}}\right)\mathbf{H}(\mu_j)\right]_{22} = 0, \quad j = 1, \ldots, 4$$

which yields

$$\mathbf{F} = \mathrm{diag}(0.0493, 0.048), \quad \mathbf{G} = \mathrm{diag}(1.8691, 1.5223).$$

The zeros, being the eigenvalues of the system grounded at the second coordinate, may be obtained by the state-space method using the gains determined above. Thus,

$$\mathbf{A} = \begin{bmatrix} \mathbf{0} & \mathbf{I} \\ -\mathbf{M}_2^{-1}\left((\mathbf{K} + \mathbf{B}\,\mathrm{diag}(g_i)\mathbf{B}^{\mathrm{T}}\right)_2 & -\mathbf{M}_2^{-1}\left((\mathbf{C} + \mathbf{B}\,\mathrm{diag}(f_i)\mathbf{B}^{\mathrm{T}}\right)_2 \end{bmatrix},$$

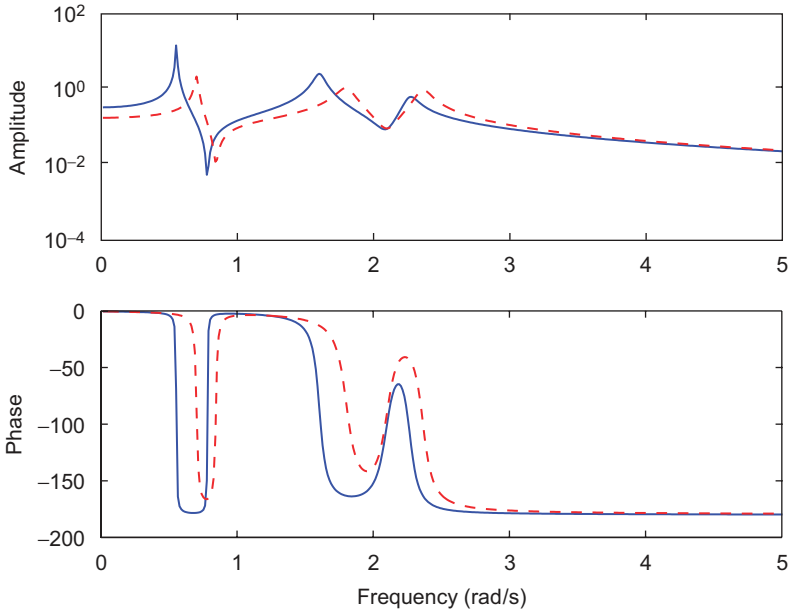

Fig. 2. Example 1—initial receptance (solid line) and modified receptance (dashed line).

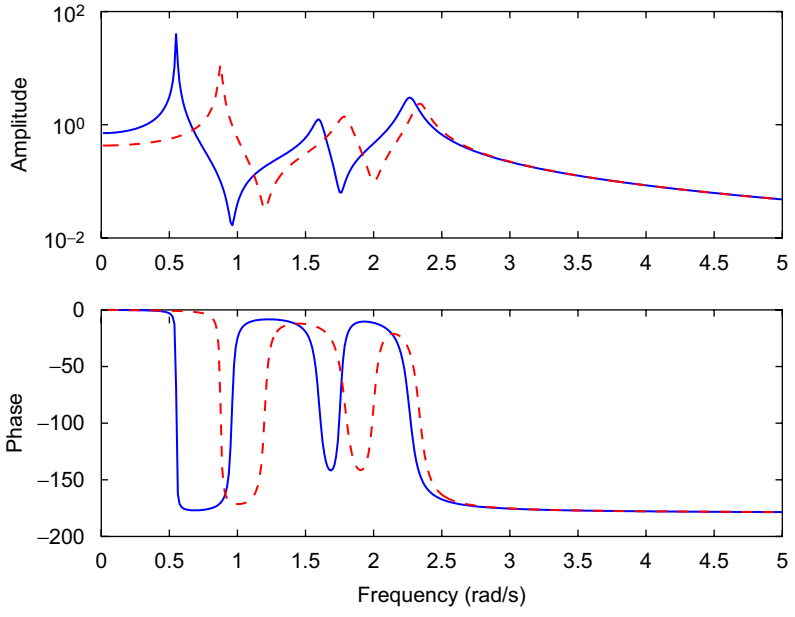

Fig. 3. Example 2—initial receptance (solid line) and modified receptance (dashed line).

where

$$\left(\mathbf{C}+\mathbf{B}\,\mathrm{diag}(f_i)\mathbf{B}^{\mathrm{T}}\right)_2=\begin{bmatrix}0.1493 & 0\\ 0 & 0.1480\end{bmatrix}$$

and

$$\left(\mathbf{K}+\mathbf{B}\,\mathrm{diag}(g_i)\mathbf{B}^{\mathrm{T}}\right)_2=\begin{bmatrix}7.8691 & -1\\ -1 & 4.5223\end{bmatrix}$$

which yields the zeros,

$$\mu_{1,2}=-0.025\pm 1.2\mathrm{i},$$
$$\mu_{3,4}=-0.037\pm 2\mathrm{i},$$

for the point receptance h_{22}. The initial and modified receptances, plotted in Fig. 3, are represented by the solid (blue) and dashed (red) lines, respectively.

Example 3 (*Assignment of poles and zeros together*). Poles and zeros are assigned to h_{11} at $\lambda_{1,2}=-0.02\pm 0.7\mathrm{i}$ and $\mu_{1,2}=-0.008\pm 0.9\mathrm{i}$, respectively. Four nonlinear equations are solved simultaneously

$$\det\left(\mathbf{I}-\mathbf{H}(\lambda_1)\mathbf{B}\,\mathrm{diag}(f_i+\lambda_1 g_i)\mathbf{B}^{\mathrm{T}}\right)=0,$$
$$\det\left(\mathbf{I}-\mathbf{H}(\lambda_2)\mathbf{B}\,\mathrm{diag}(f_i+\lambda_2 g_i)\mathbf{B}^{\mathrm{T}}\right)=0,$$
$$\left[\mathrm{adj}\left(\mathbf{I}+\mathbf{H}(\mu_1)\mathbf{B}\,\mathrm{diag}(g_i+\mu_1 f_i)\mathbf{B}^{\mathrm{T}}\right)\mathbf{H}(\mu_1)\right]_{11}=0,$$
$$\left[\mathrm{adj}\left(\mathbf{I}+\mathbf{H}(\mu_2)\mathbf{B}\,\mathrm{diag}(g_i+\mu_2 f_i)\mathbf{B}^{\mathrm{T}}\right)\mathbf{H}(\mu_2)\right]_{11}=0$$

which yields to the following gains:

$$\mathbf{F}=\mathrm{diag}(0.4023,0.0404),\quad \mathbf{G}=\mathrm{diag}(0.3720,0.6836).$$

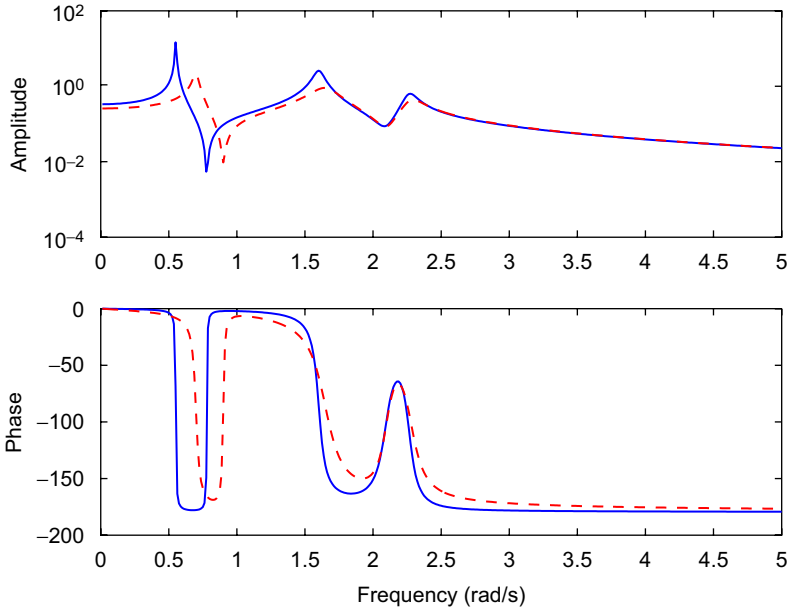

Fig. 4. Example 3—initial receptance (solid line) and modified receptance (dashed line).

State-space analysis, using these gains, results in the poles,

$$\lambda_{1,2} = -0.0200 \pm 0.7000\mathrm{i},$$
$$\lambda_{3,4} = -0.0992 \pm 1.6497\mathrm{i},$$
$$\lambda_{5,6} = -0.0798 \pm 2.2755\mathrm{i}$$

and zeros,

$$\mu_{1,2} = -0.0080 \pm 0.9000\mathrm{i},$$
$$\mu_{3,4} = -0.0654 \pm 2.1007\mathrm{i}.$$

The initial and modified receptances h_{11} are plotted in Fig. 4, represented by the solid (blue) and dashed (red) line, respectively.

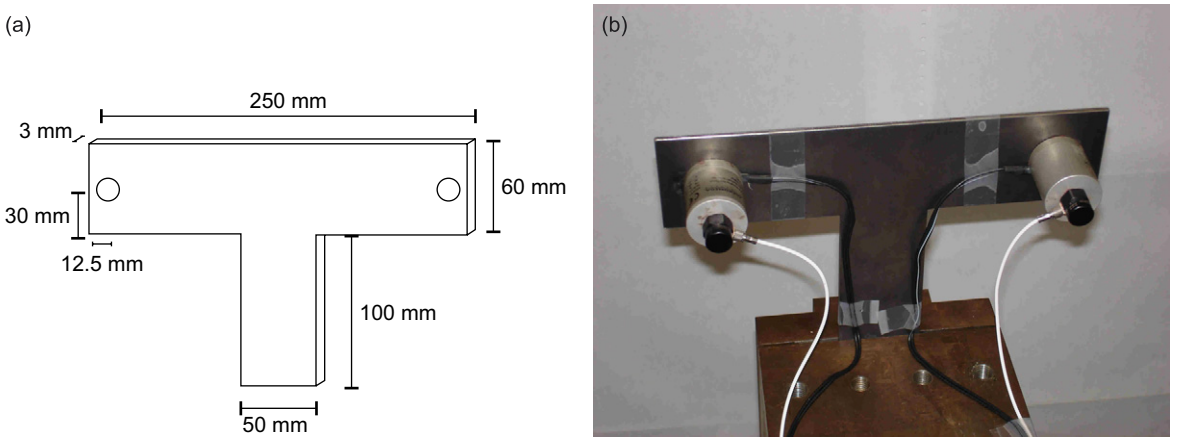

Fig. 5. T-shaped plate: (a) dimensions and (b) experimental arrangement.

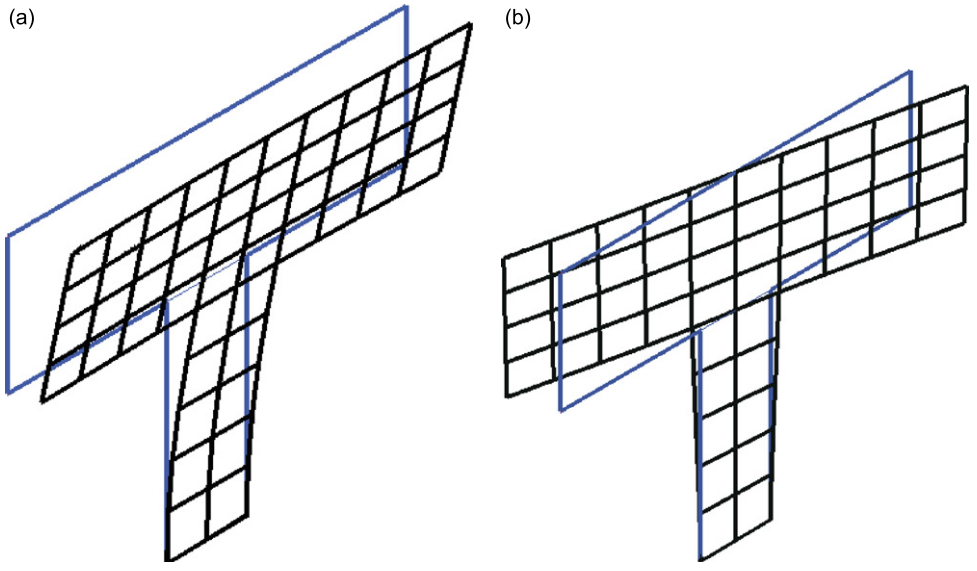

Fig. 6. (a) First mode (stem bending) and (b) second mode (stem twisting).

5. Experimental examples

Experiments were carried out on the T-shaped plate shown in Fig. 5 using two sets of collocated sensors (Kistler accelerometer type 8636C50) and inertial actuators (Micromega Dynamics type IA-01). The internal active damper that forms part of the inertial actuator, based on analogue integration of acceleration was not used. Instead, signals from the Kistler accelerometers were integrated twice by digital means, thereby enabling both velocity and displacement feedback, implemented using MATLAB/Simulink and dSPACE. Open-loop receptances were measured by means of a modal test using hammer excitation with the inertial actuators in place but not operational. The H_1 estimator was applied using the following test parameters: sample rate 256 Hz, frequency resolution 0.125 Hz, number of hits 20 and an exponential window with a decay to 1% applied to the measured accelerations. The first two natural frequencies of the open-loop system were at 40 Hz (252 rad/s) and 52 Hz (325 rad/s). The first mode was a stem bending mode and the second showed stem twisting with the two arms in anti-phase. The third natural frequency, in-phase arm bending, occurred at 125 Hz (785 rad/s) some distance away from the first two modes. The first two mode shapes are shown in Fig. 6.

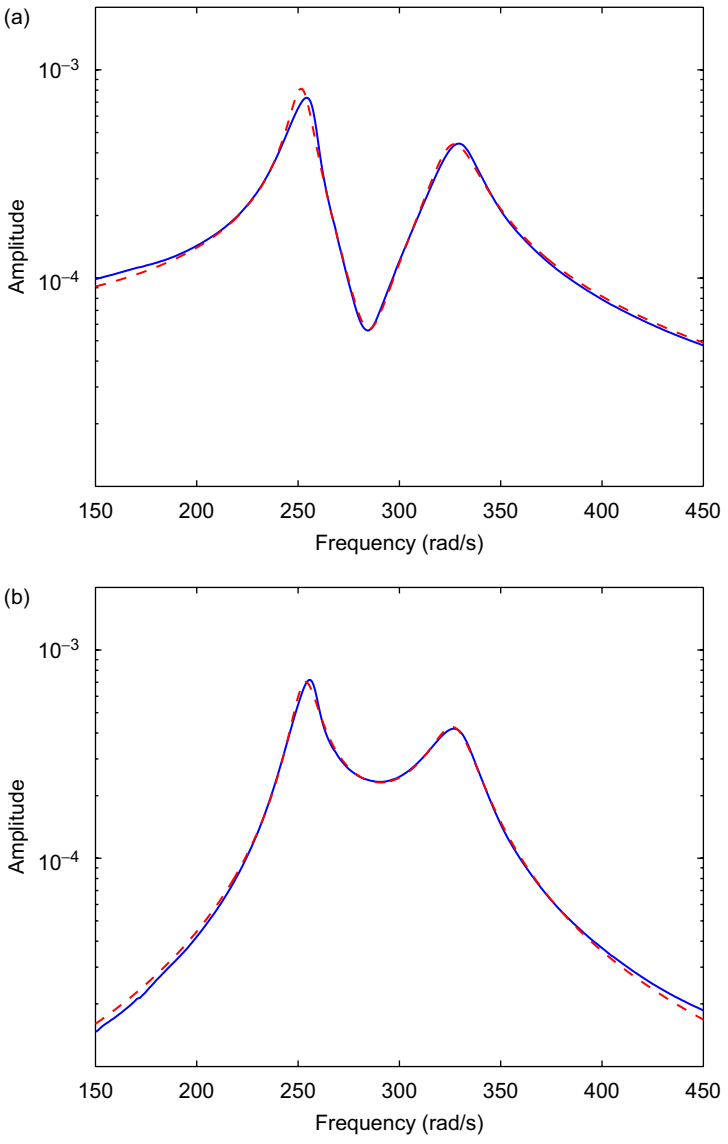

Fig. 7. Rational fraction curve fit (a) $h_{11}(i\omega)$, (b) $h_{12}(i\omega)$ measurement—solid line; fitted curve—dashed line.

The purpose of using receptances instead of the **M**, **C**, **K** matrices is that uncertainties, approximations and assumptions associated with finite element models are avoided completely. However $\mathbf{H}(\mathrm{i}\omega)$ is available from vibration experiments and not $\mathbf{H}(s)$, as required by the theory. Rational fraction polynomials were fitted to the measured terms in $\mathbf{H}(\mathrm{i}\omega)$ and the coefficients of the numerator and denominator polynomials determined [29]. The coefficients were found by solving a least-squares problem, which should be well conditioned so that the coefficients are not sensitive to small changes in the measurements. The receptances $h_{11}(\mathrm{i}\omega)$ and $h_{22}(\mathrm{i}\omega)$ were almost identical because of geometric symmetry of the T-plate and due to linearity $h_{12}(\mathrm{i}\omega)$ and $h_{21}(\mathrm{i}\omega)$ were found to be very similar. The fitted receptances are presented in Fig. 7 where measurements are represented by full lines (blue) and fitted curves are shown as dashed lines (red). The good agreement shown in

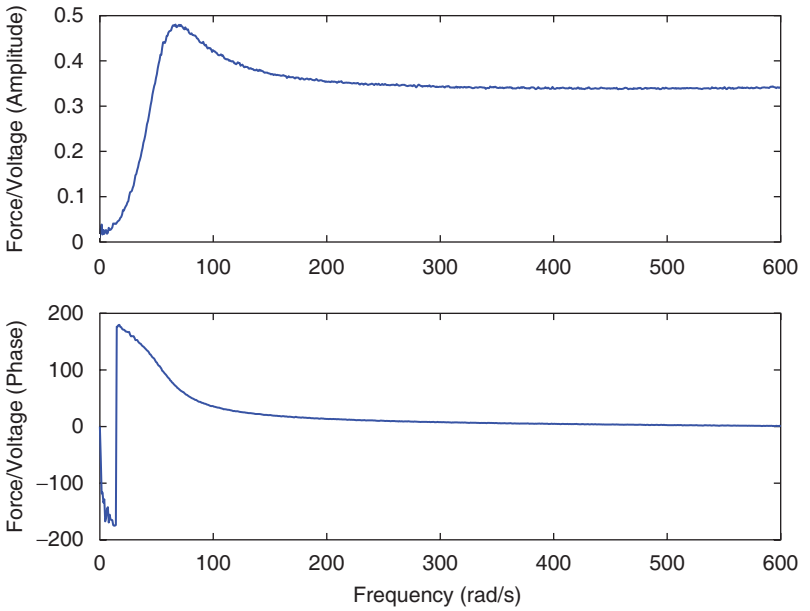

Fig. 8. Actuator force–voltage transfer function.

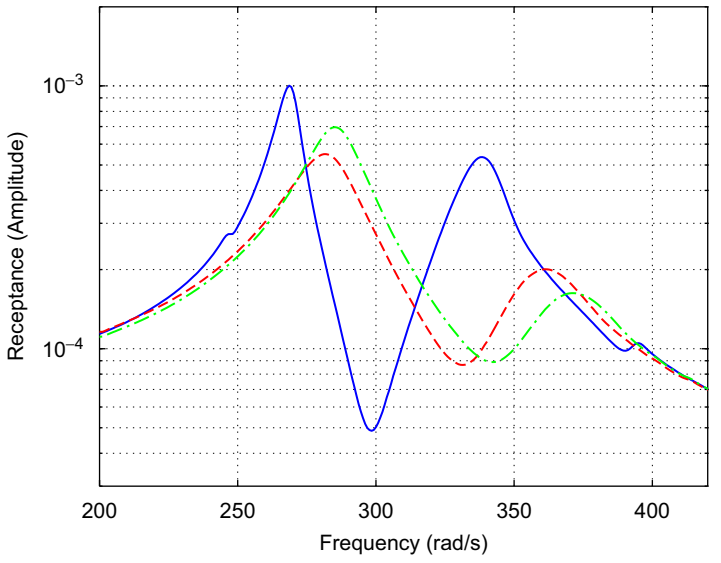

Fig. 9. Assignment of poles. Solid line: open-loop receptance. Dashed line: closed-loop receptance for the first test. Dot-dashed line: closed-loop receptance for the second test.

Fig. 7, for amplitude, was similarly obtained for phase. The following polynomials were identified:

$$h_{11}(s) = h_{22}(s) = \frac{7.956 \times 10^{-10}s^2 + 1.382 \times 10^{-8}s + 6.438 \times 10^{-5}}{1.476 \times 10^{-10}s^4 + 4.987 \times 10^{-9}s^3 + 2.515 \times 10^{-5}s^2 + 0.0003862s + 1},$$

$$h_{12}(s) = h_{21}(s) = \frac{-1.334 \times 10^{-10}s^2 - 4.678 \times 10^{-9}s + 5.208 \times 10^{-6}}{1.476 \times 10^{-10}s^4 + 4.987 \times 10^{-9}s^3 + 2.515 \times 10^{-5}s^2 + 0.0003862s + 1}.$$

It should be pointed out that the rational fraction polynomials represent a model of the system. However all that is required of this model is that it is accurate at the chosen location of the poles and zeros to be assigned. In the case of lightly damped systems it is likely that the identified rational fraction polynomial will be accurate if the curve fit agrees closely with the measured terms in $\mathbf{H}(i\omega)$.

An expression for the force–voltage transfer function of an inertial actuator with a fixed base is given by Preumont [27]. Above a critical frequency it is shown that the actuator behaves as an ideal force generator

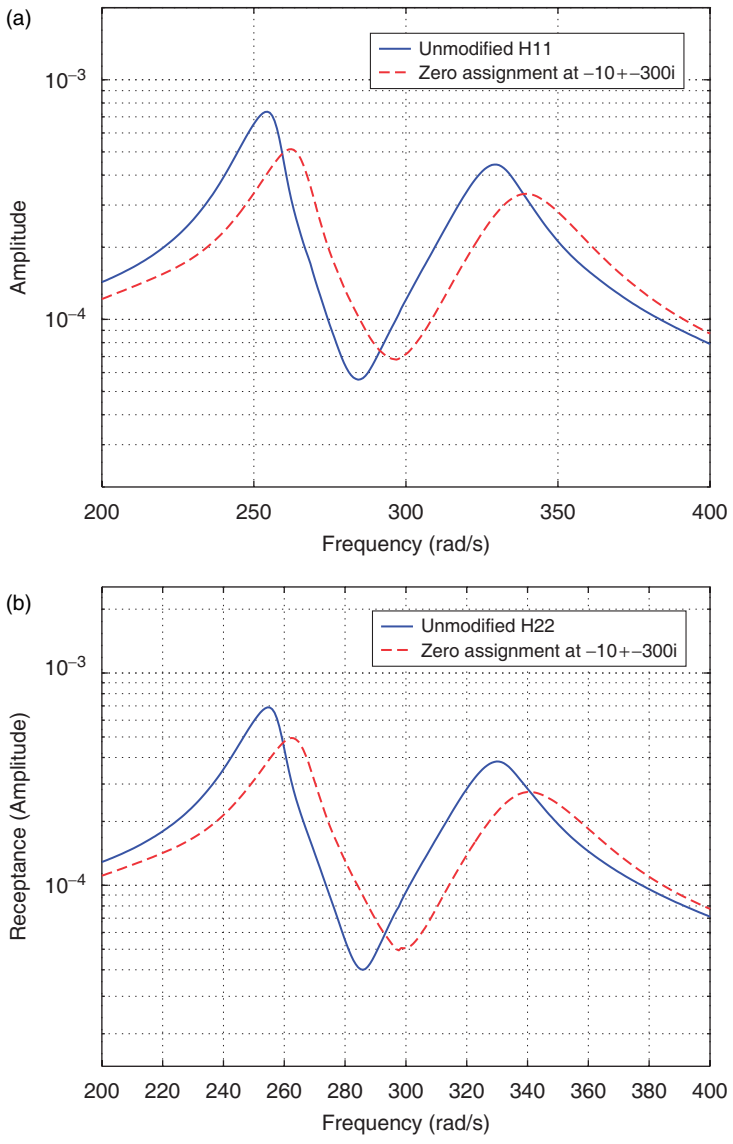

Fig. 10. Assignment of zeros: (a) h_{11} and (b) h_{22}.

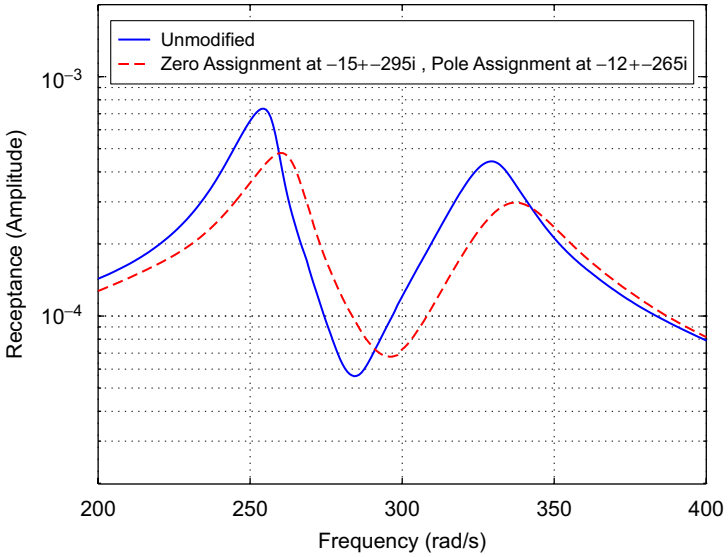

Fig. 11. Simultaneous assignment of poles and zeros.

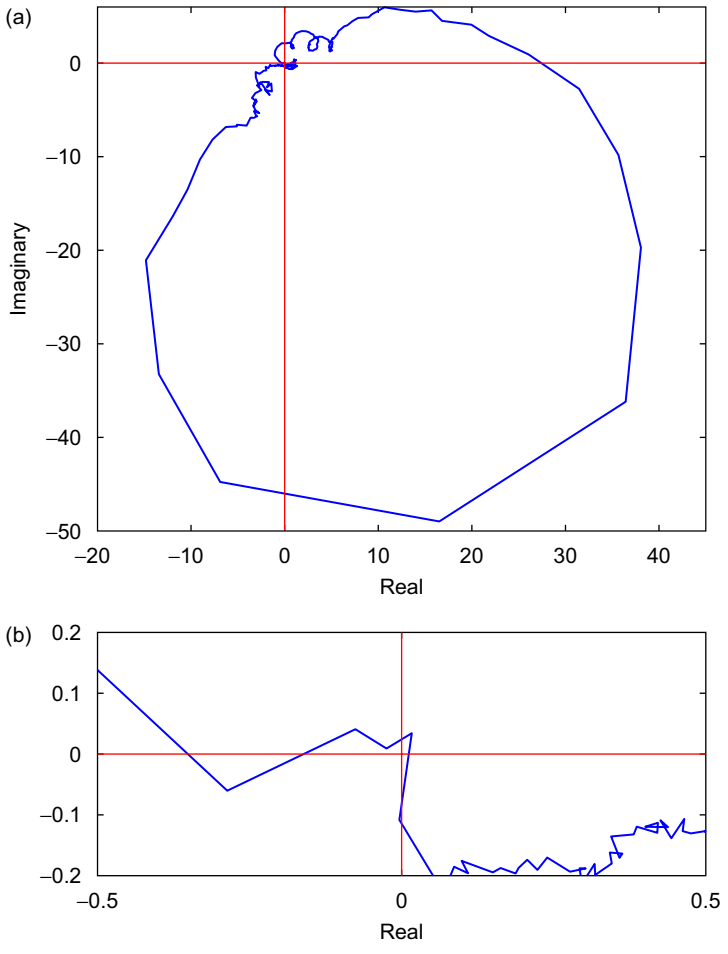

Fig. 12. Polar plot of $\det[\mathbf{I}+0.37\times\mathbf{H}(i\omega)\mathbf{B}\ \mathrm{diag}(g_i+i\omega f_i)\mathbf{B}^{\mathrm{T}}]$: (a) full polar plot and (b) magnified view close to the origin.

with constant amplitude and zero phase. This is the case shown in Fig. 8, the force being measured by a force sensor inserted between the base of the actuator and a heavy rigid mass. Preumont's analysis is in fact a simplification of the real situation since the actuator was fixed to the flexible T-plate in our control application. However a small distance away from the T-plate resonances the expression was found to hold good. A gain of 0.37 was obtained from the curve shown in Fig. 8, being the average value of the almost constant pure gain (zero phase) at frequencies greater than the natural frequency of the actuator at around 65 rad/s.

Experiment 1 (*Assignment of poles*). Poles were firstly assigned at $\lambda_{1,2} = -12 \pm 284\mathrm{i}$ and $\lambda_{3,4} = -22 \pm 365\mathrm{i}$ and then in a second test at $\lambda_{1,2} = -10 \pm 290\mathrm{i}$ and $\lambda_{3,4} = -25 \pm 375\mathrm{i}$. In all of the three experiments the force and sensor distribution matrices were set to $\mathbf{B} = \mathbf{D}^{\mathrm{T}} = \mathbf{I}$, where $\mathbf{I}$ denotes the identity matrix. In the first test, gains with the values of $\mathbf{G} = \mathrm{diag}(205,10955)$ and $\mathbf{F} = \mathrm{diag}(4.4,11.8)$ were found and in the second test $\mathbf{G} = \mathrm{diag}(124,14339)$ and $\mathbf{F} = \mathrm{diag}(0.5,11.19)$. Fig. 9 shows experimental receptances for the open-loop system as the full line (blue) and closed-loop receptances, h_{11}, for the first and second tests. The receptance for the first test is shown as a dashed line (red) and for the second test as a dot-dashed line (green). As expected, the peaks of the dashed and dot-dashed lines can be seen to agree very well with the imaginary parts of the assigned poles for the first and second test, respectively. The actuators were operational during the closed-loop modal tests used to determine the receptances from excitation by an instrumented hammer.

Experiment 2 (*Assignment of zeros*). To maintain geometrical symmetry of the T-plate identical zeros were assigned to h_{11} and h_{22} at $\mu_1,\mu_2 = -10 \pm 300\mathrm{i}$. Gains were determined as $\mathbf{F} = 1.8\mathbf{I}$, $\mathbf{G} = 3735\mathbf{I}$. Experimental open-loop and closed-loop receptances are shown in Fig. 10 where the frequency of the zeros is seen to agree very well with the assigned value of 300 rad/s and the poles remain stable.

Experiment 3 (*Simultaneous assignment of poles and zeros*). Poles and zeros were assigned to h_{11} at $\lambda_{1,2} = -15 \pm 295\mathrm{i}$ and $\mu_{1,2} = -12 \pm 265\mathrm{i}$, respectively. Gain values of $\mathbf{G} = \mathrm{diag}(3720,\ 2355)$ and $\mathbf{F} = \mathrm{diag}(2.24,\ 5.75)$ were found and the resulting open-loop and closed-loop receptances were found as shown in Fig. 11. It can be seen in Fig. 11 that the frequencies of the first peak and dip of the dashed (red) line, that represents the closed-loop receptance, agree closely with the imaginary part of the assigned poles and zeros.

5.1. Stability robustness

In this section the stability robustness of the experimental T-plate structure to active vibration control by pole-zero placement is addressed. The problem considered is that of Example 2 in Section 4 above, namely the assignment of zeros of h_{11} and h_{22} to $\mu_1,\mu_2 = -10 \pm 300\mathrm{i}$. The open-loop transfer function between the input

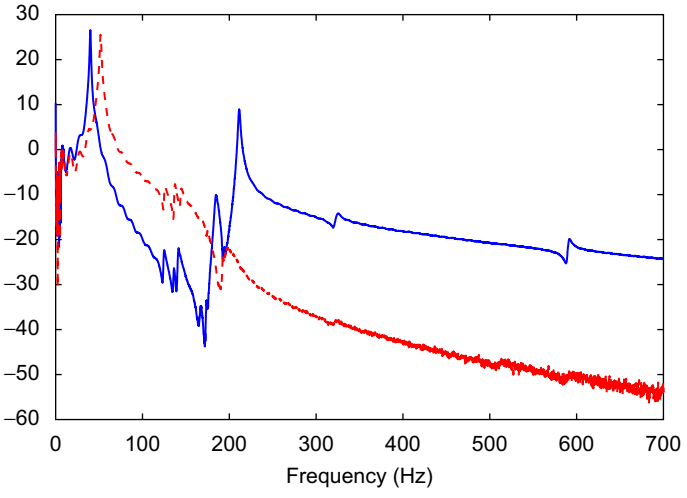

Fig. 13. Spectrum of eigenvalues λ_1 (dashed line) and λ_2 (solid line) of the open-loop transfer function $0.37 \times \mathbf{H}(\mathrm{i}\omega)\mathbf{B}\ \mathrm{diag}(g_i + \mathrm{i}\omega f_i)\mathbf{B}^{\mathrm{T}}$.

voltage to the actuators and the output displacement $\mathbf{y}(s)$ is then defined as $0.37 \times \mathbf{H}(s)\mathbf{B}\ \mathrm{diag}(g_i + sf_i)\mathbf{B}^{\mathrm{T}}$, where the gain of 0.37 represents the actuator dynamic as described previously.

Open-loop experiments were carried out by applying random voltages to the actuators in the range of 0–1000 Hz and measuring the output voltages, calibrated for displacement, from the dSPACE board. The frequency-domain requirements for the stability of single-input–single-output (SISO) systems take the form of the standard Nyquist criterion and in the MIMO case they involve its multivariable generalisation [30]. Thus the system may be considered stable if $\det[\mathbf{I} + 0.37 \times \mathbf{H}(\mathrm{i}\omega)\mathbf{B}\ \mathrm{diag}(g_i + \mathrm{i}\omega f_i)\mathbf{B}^{\mathrm{T}}]$, $0 < \omega < \infty$, does not enclose the point (0, 0). It can be seen from Figs. 12(a) and (b) that this appears to be the case, although the system is extremely close to being marginally stable. The spectrum in Fig. 13 shows good roll-off of the eigenvalues λ_1 and λ_2 of the open-loop transfer function, indicated by the dashed line (red) and solid line (blue), respectively, thereby confirming that in practice spillover does not lead to instability at higher frequencies.

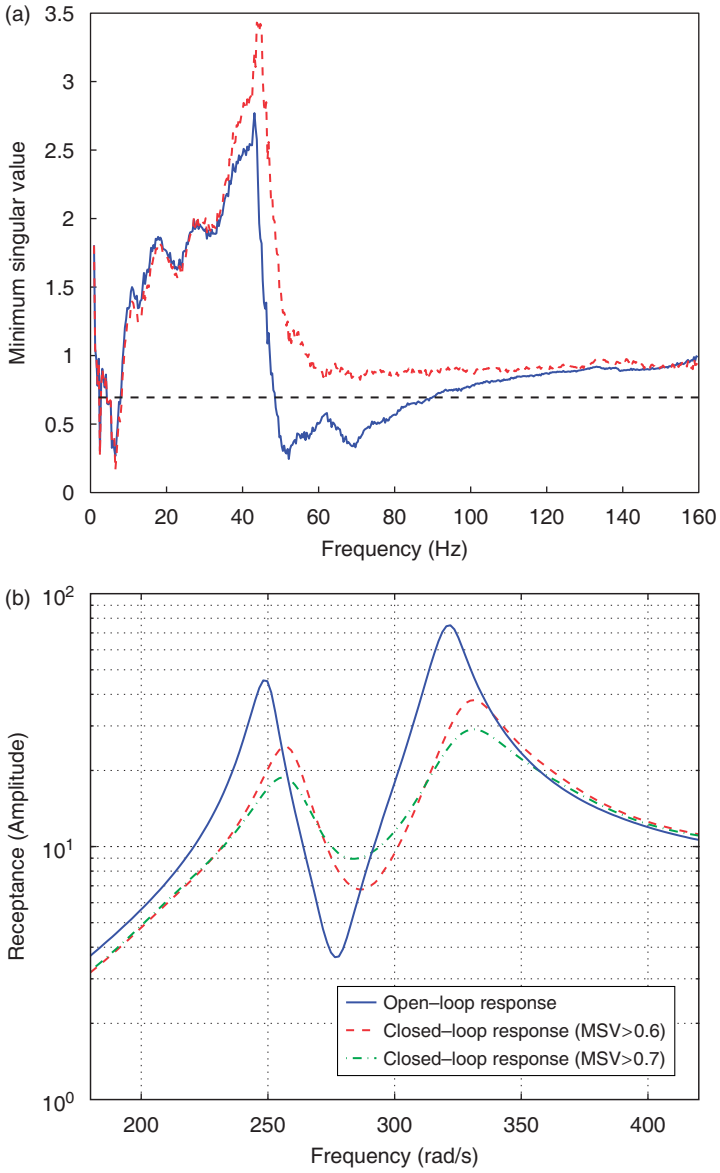

Fig. 14. Robustness (a) minimum singular value. Solid line—without constraint; dashed line—after added constraint. (b) Receptance. Solid line—open-loop receptance; dashed line—closed-loop receptance for $\underline{\sigma} > 0.6$ from 50 to 100 Hz; dot-dashed line—closed-loop receptance for $\underline{\sigma} > 0.7$ from 50 to 100 Hz.

The robustness of the closed-loop system can be improved by increasing the minimum singular value $\underline{\sigma}$ of $[\mathbf{I}+0.37\times\mathbf{H}(s)\mathbf{B}\ \mathrm{diag}(g_i+sf_i)\mathbf{B}^{\mathrm{T}}]$ as explained by Maciejowski [31], thereby defining the following constraint:

$$\underline{\sigma}\left[\mathbf{I}+0.37\times\mathbf{H}(s)\mathbf{B}\,\mathrm{diag}(g_i+sf_i)\mathbf{B}^{\mathrm{T}}\right]>r$$

on the solution of the nonlinear characteristic equations.

In our particular example, a constraint of $\underline{\sigma}>0.7$ was applied over the frequency range of 50–100 Hz. The resulting control gains were found to be,

$$\mathbf{F}=\begin{bmatrix}12.7 & 0\\ 0 & 13.8\end{bmatrix},\quad \mathbf{G}=\begin{bmatrix}3734.9 & 0\\ 0 & 3734.9\end{bmatrix}.$$

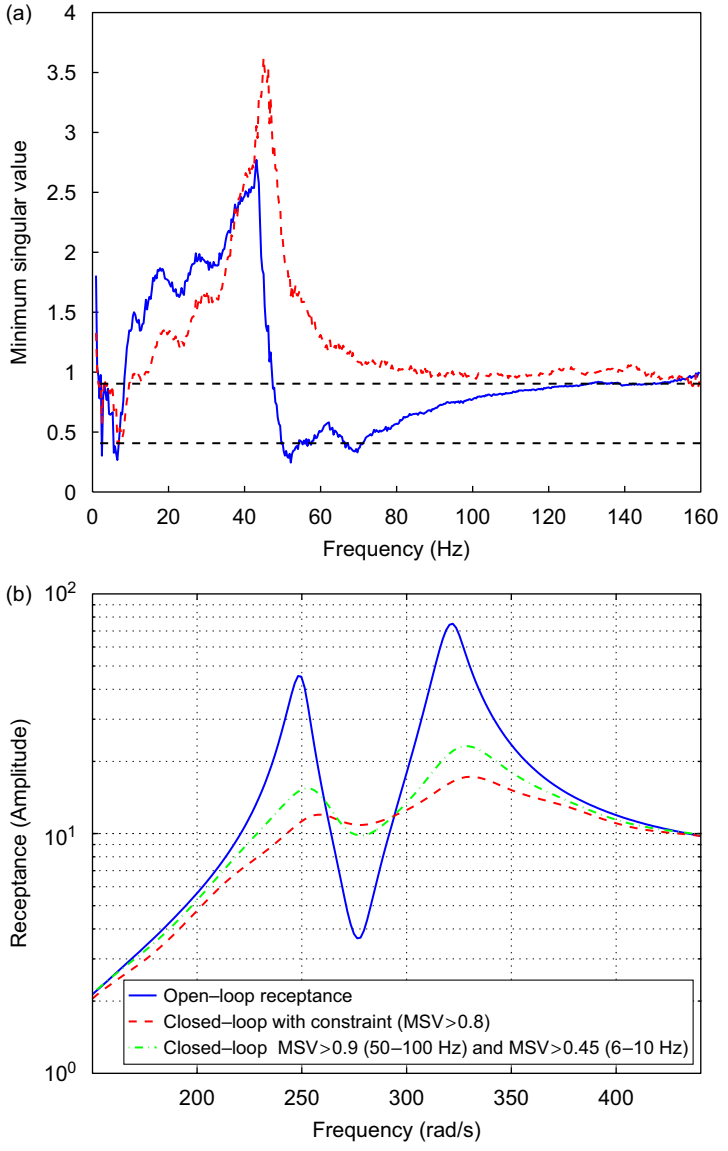

Fig. 15. Robustness (a) minimum singular value. Solid line—without constraint; dashed line—after added constraint. (b) Receptance. Solid line—open-loop receptance; dashed line—closed-loop receptance for $\underline{\sigma}>0.8$ from 50 to 100 Hz; dot-dashed line—closed-loop receptance for $\underline{\sigma}>0.9$ from 50 to 100 Hz and $\underline{\sigma}>0.45$ from 6 to 10 Hz.

In Fig. 14(a) the solid (blue) line denotes $\underline{\sigma}$ versus frequency without constraint. The dashed (red) line is the case of $\underline{\sigma} > 0.7$ for the range of 50–100 Hz. A series of modal tests using hammer excitation were carried out with the feedback control gains obtained with the added constraints $\underline{\sigma} > 0.6$ and 0.7. The solid (blue) line in Fig. 14(b) represents the unconstrained open-loop receptance. The dashed (red) and dot-dashed (green) lines represent the closed-loop receptances after the added constraints $\underline{\sigma} > 0.6$ and 0.7 were applied over the range of 50–100 Hz. It is seen that the effect of the constraints is to add damping and thereby improve the stability robustness of the T-plate system. Of course, this is achieved at the cost of reduced accuracy in the placement of the zeros.

A further constraint, $\underline{\sigma} > 0.45$, was then added to the range 6–10 Hz to address the sharp 'dip' in the dashed line of Fig. 14(a) at low frequencies. In the range 50–100 Hz the lowest singular value was constrained such that $\underline{\sigma} > 0.9$. Control gains were then obtained as

$$\mathbf{F} = \begin{bmatrix} 17.35 & 0 \\ 0 & 22.64 \end{bmatrix}, \quad \mathbf{G} = \begin{bmatrix} 1709.5 & 0 \\ 0 & 2164 \end{bmatrix}.$$

Fig. 15 shows the minimum singular values and the closed-loop receptances for the system, now with two constraints. This results in considerably increased damping over the previous test and further deterioration in the accuracy of placing the zeros.

6. Conclusions

Active vibration suppression by eigenvalue assignment using output feedback and the receptance method is presented. The method does not require the usual **M**, **C**, **K** matrices but uses measured receptances from the open-loop system instead. Illustrative numerical examples are presented, as are the results of a physical experiment using collocated inertial actuators and accelerometers, to assign poles and zeros (natural frequencies and anti-resonances). In the experiments, receptances $\mathbf{H}(s)$ are determined from the measured $\mathbf{H}(\mathrm{i}\omega)$ by fitting rational fraction polynomials. Closed-loop receptances, obtained by applying gains determined from the analysis, have peaks and dips that agree very closely with the imaginary parts of the assigned poles and zeros. The stability robustness may be improved by applying a constraint to the singular values of the matrix return difference.

Acknowledgements

The authors wish to acknowledge helpful conversations with Professor P. Gardonio (Southampton University), Dr. A.T. Shenton (Liverpool University), Dr. R. Stanway (Sheffield University) and Professor G.-F. Yao (Jilin University).

References

[1] W.M. Wonham, On pole assignment in multi-input controllable linear systems, *IEEE Transactions on Automatic Control* AC-12 (1967) 660–665.
[2] E.J. Davison, On pole assignment in linear systems with incomplete state feedback, *IEEE Transactions on Automatic Control* AC-15 (1970) 348–351.
[3] H. Kimura, Pole assignment by gain output feedback, *IEEE Transactions on Automatic Control* AC-20 (1975) 509–516.
[4] B.C. Moore, On the flexibility offered by state feedback in multivariable systems beyond closed loop eigenvalue assignment, *IEEE Transactions on Automatic Control* AC-21 (1976) 689–692.
[5] J. Kautsky, N.K. Nichols, P. Van Dooren, Robust pole assignment in linear state feedback, *International Journal of Control* 41 (5) (1985) 1129–1155.
[6] B.N. Datta, S. Elhay, Y.M. Ram, Orthogonality and partial pole placement for the symmetric definite quadratic pencil, *Linear Algebra and its Applications* 257 (1997) 29–48.
[7] I. Bucher, S. Braun, The structural modification inverse problem, *Mechanical Systems and Signal Processing* 7 (1993) 217–238.
[8] J.E. Mottershead, C. Mares, M.I. Friswell, An inverse method for the assignment of vibration nodes, *Mechanical Systems and Signal Processing, Special Issue on Inverse Methods in Structural Dynamics* 15 (1) (2001) 87–100.
[9] J.E. Mottershead, Structural modification for the assignment of zeros using measured receptances, *Transactions of the American Society of Mechanical Engineers, Journal of Applied Mechanics* 68 (5) (2001) 791–798.

[10] J.E. Mottershead, A. Kyprianou, H. Ouyang, Structural modification, part 1: rotational receptances, *Journal of Sound and Vibration* 284 (1–2) (2005) 249–265.
[11] A. Kyprianou, J.E. Mottershead, H. Ouyang, Structural modification, part 2: assignment of natural frequencies and antiresonances by an added beam, *Journal of Sound and Vibration* 284 (1–2) (2005) 267–281.
[12] J.E. Mottershead, M.G. Tehrani, D. Stancioiu, S. James, H. Shahverdi, Structural modification of a helicopter tailcone, *Journal of Sound and Vibration* 298 (1–2) (2006) 366–384.
[13] J.E. Mottershead, Y.M. Ram, Inverse eigenvalue problems in vibration absorption: passive modification and active control, *Mechanical Systems and Signal Processing* 20 (1) (2006) 5–44.
[14] L. Benassi, S.J. Elliott, P. Gardonio, Active vibration isolation using an inertial actuator with local force feedback control, *Journal of Sound and Vibration* 276 (2004) 157–179.
[15] R.L. Clark, W.R. Saunders, G.P. Gibbs, *Adaptive Structures, Dynamics and Control*, Wiley/Interscience, New York, 1998.
[16] P. Gardonio, E. Bianchi, S.J. Elliot, Smart panel with multiple decentralised units for the control of sound transmission. Part I: theoretical predictions, *Journal of Sound and Vibration* 274 (2004) 163–192.
[17] P. Gardonio, E. Bianchi, S.J. Elliot, Smart panel with multiple decentralised units for the control of sound transmission. Part II: design of decentralised control units, *Journal of Sound and Vibration* 274 (2004) 193–213.
[18] E. Bianchi, P. Gardonio, S.J. Elliot, Smart panel with multiple decentralised units for the control of sound transmission. Part III: control system implementation, *Journal of Sound and Vibration* 274 (2004) 215–232.
[19] R. Stanway, J.A. Rongong, N.D. Sims, Active constrained layer damping: a state-of-the-art review, *Proceedings of the IMechE, Part I, Journal of Systems and Control* 217 (6) (2003) 437–456.
[20] M.J. Balas, Feedback control of flexible structures, *IEEE Transactions on Automatic Control* AC-23 (1978) 673–679.
[21] L. Meirovitch, *Dynamics and Control of Structures*, Wiley, New York, 1990.
[22] K. Jian, M.I. Friswell, Designing distributed modal sensors for plate structures using finite element analysis, *Mechanical Systems and Signal Processing* 20 (8) (2006) 2290–2304.
[23] F. Tisseur, K. Meerbergen, The quadratic eigenvalue problem, *SIAM Review* 43 (2) (2001) 235–286.
[24] Y.-H. Lim, S.V. Gopinathan, V.V. Varadan, V.K. Varadan, Finite element simulation of smart structures using an output feedback controller for vibration and noise control, *Smart Materials and Structures* 8 (1999) 324–337.
[25] U. Stobener, L. Gaul, Active vibration control of a car body based on experimentally evaluated modal parameters, *Mechanical Systems and Signal Processing* 15 (1) (2001) 173–188.
[26] Y.M. Ram, J.E. Mottershead, Receptance method in active vibration control, *American Institute of Aeronautics and Astronautics Journal* 45 (3) (2007) 562–567.
[27] A. Preumont, *Vibration Control of Active Structures*, second ed., Kluwer Academic Publishers, Dordrecht, 2002.
[28] C.R. Fuller, S.J. Elliot, P.A. Nelson, *Active Control of Vibration*, Academic Press, San Diego, 1996.
[29] D. Formenti, M. Richardson, Parameter estimation from frequency response measurements using rational fraction polynomials, *Proceedings of the First International Modal Analysis Conference*, Orlando, FL, 1982.
[30] H.H. Rosenbrock, The stability of multivariable systems, *IEEE Transactions on Automatic Control* AC17 (1972) 105–107.
[31] J.M. Maciejowski, *Multivariable Feedback Design*, Addison-Wesley, Wokingham, England, 1989.